Experimental study on long spanning composite cellular beam under flexure and shear

Experimental study on long spanning composite cellular beam under flexure and shear

Therese Sheehan[a*], Xianghe Dai[a], Dennis Lam[a], Eleftherios Aggelopoulos[b], Mark Lawson[b], Renata Obiala[c]

[a] University of Bradford, School of Engineering, United Kingdom
t.sheehan@bradford.ac.uk, x.dai@bradford.ac.uk, d.lam1@bradford.ac.uk
[b] The Steel Construction Institute (SCI), United Kingdom
e.aggelopoulos@steel-sci.com, m.lawson@steel-sci.com
[c] ArcelorMittal R&D, Luxembourg
renata.obiala@arcelormittal.com

Abstract

This paper describes a sequence of experiments on a long-span asymmetric composite cellular beam. This type of beam has become very popular, combining the composite action between the steel and concrete with the increased section depth, compared with more commonly used solid-web I sections. Openings in the steel web also reduce the self-weight and can accommodate the passage of service ducts. Eurocode 4 recommends a high degree of shear connection for asymmetric composite beams despite the practical difficulties in achieving this. Recent research suggests that the required degree of shear connection could be reduced, particularly for beams that are unpropped during construction. However, little test data exists to verify the behaviour of unpropped composite cellular beams. Therefore two series of tests were conducted on a 15.26 m long asymmetric composite cellular beam with regular circular openings and an elongated opening at the mid-span. The degree of shear connection was 36%, less than half of that recommended in Eurocode 4, and the beam was unpropped during construction. The beam was subjected to uniformly distributed loading and shear load during the tests. The end-slip, mid-span vertical deflection, shear connector capacity and strain distribution were examined. The beam failed at an applied uniform load of 17.2 kN/m^2 (3.4 × design working load 5.0 kN/m^2). The member withstood an applied shear load that was 45% higher than predicted, and exhibited a Vierendeel mechanism at the elongated opening. Overall, these tests demonstrated the potential of unpropped composite cellular beams with low degrees of shear connection.

Keywords

composite beams; shear connection; cellular beams; experiments; unpropped construction; Eurocode 4

*corresponding author, tel: +44 (0)1274235779; email: t.sheehan@bradford.ac.uk

1 Introduction

Composite beams, consisting of steel I-beams connected to concrete slabs, are a popular choice in structures around the world. The composite action is achieved between the components through the use of shear connectors, increasing the member stiffness and loading-bearing capacity and enabling the member to span long distances between supports. Cellular beams, consisting of regular circular openings in the web, are also widely used for long spans. These are formed by cutting and re-welding two steel I-sections, typically providing a beam with a greater cross-section depth than the parent members. This is a highly efficient system that combines an increase in bending resistance with a reduction in material and member self-weight. The web-openings are aesthetically pleasing and enable the passage of service ducts to reduce the structural zone.

In recent years this relatively new form of asymmetric steel-concrete composite cellular beam has been used extensively in construction practice. Since the top flange acts compositely with the slab, the bottom part of the cellular beam is cut from a heavier section than the top part to improve the design efficiency. The ratio of the bottom to top flange areas is usually in the range of 1.5 to 2.5. Extensive research has been conducted to date on composite beams and cellular beams. Ranzi *et al*. [1] carried out full scale tests on composite beams with deep trapezoidal decking. Lam [2] examined the resistance of headed shear studs when used in composite beams in conjunction with precast hollow core slabs. Erdal and Saka [3] carried out laboratory tests to establish the load-carrying capacity of non-composite cellular steel beams. Chung *et al*. [4] conducted an analytical study of non-composite cellular beams, focussing on the Vierendeel mechanism that occurred at the web opening. Research has also been carried out in recent years on the new type of composite cellular beams. Lawson *et al*. [5] considered the design rules for composite asymmetric cellular beams and verified these rules using finite element analysis. However, very little test data currently exists to support the design of asymmetric composite cellular beams, in particular longer span composite cellular beams. A European research project called “LWO” [6] included 3 tests on composite cellular beams spanning 7.2 m but only one of these beams was asymmetric. In Eurocode 4 [7], a higher degree of shear connection is

required for asymmetric beams than for symmetric beams. If is often impossible to achieve the desired degree of shear connection (nearly 100%), since this is limited by the spacing of the deck ribs (usually 300 mm for trapezoidal decking). Furthermore, the development of deeper deck profiles has increased the spacing between beams from 3 m to 4.5 m, increasing the potential load to be transferred by shear studs. Hence design is often governed by achieving the minimum degree of shear connection.

Composite beams may be constructed with or without the use of temporary props. If props are used, the weight of the steel beam and fresh concrete of the slab is supported by the props. Once the slab concrete has gained sufficient strength, the props are removed and the composite section bears the self-weight. Without the use of props during the concrete slab casting, the self-weight of the beam and the wet concrete is supported by the steel beam alone, since the concrete does not have adequate strength at this stage. Unpropped construction is popular since it reduces the time and operational cost during construction, but as suggested by Lawson and Saverirajan [8] and Banfi [9], there are differences in response between propped and unpropped beams. Unpropped beams experience a lower degree of end-slip and require a lower degree of shear connection. However, the advantages of unpropped beams are not currently exploited in Eurocode 4.

Some noteworthy differences exist between cellular beams and I beams with solid webs. Owing to the presence of web openings, cellular beams do not need to develop plasticity over the full depth of the cross-section. Hence lower strains occur in the steel section under bending and the end-slip between steel and concrete is reduced. A Vierendeel mechanism can occur at the web openings and hence the beam is not required to resist the full plastic bending resistance. The design of long-span cellular beams is usually governed by the deflections or natural frequency at the serviceability limit state. Taking these differences into consideration, and to address some of the aforementioned issues, a 15.26m composite cellular beam was tested as part of the European research project “Development of Improved Rules for Shear Connection in Composite Beams (DISCCO)” at the University of Bradford, UK. The main purposes of this test are to investigate:

- The ability of the concrete steel composite beam to develop its plastic bending resistance with low degrees of shear connection (less than the required limit given in the Eurocode 4);
- The effect of un-propped construction on the longitudinal shear connector forces;
- The effect of partial shear connection and the regular openings on the additional deflection of composite beam;
- An improvement in the local composite action on the Vierendeel bending resistance at circular and elongated openings.

2 Composite Beam Details

2.1 Geometry and components

The cellular beam spanned 15.26m between the supports and comprised two structural steel sections. The top T-section was 305 mm deep and cut from an IPE 450 section, while the bottom T-section was 260 mm deep came from a HEB 360 section, providing a total cross-section depth of 565 mm and a length-to-depth ratio of 27 (15.26/0.565). Hence the beam was highly asymmetric with a bottom flange area to top flange area ratio of 2.43. The diameter of the cell openings is 425 mm with a centre-to-centre spacing of 680 mm. The cross-section dimensions are shown in Figure 1. A trapezoidal deck profile was used to support the concrete slab, with the deck ribs running in the transverse direction to the beam length, and shear connectors in the ribs to connect the slab and steel beam. According to Clause 6.6.5.5 in EN 1994-1-1 (2004), if the shear connector spacing exceeds $15t_f\sqrt{235/f_y}$ in this type of arrangement, where t_f is the thickness of the top flange and f_y is the material yield strength, then the beam cross-section should be classified in the same manner as a steel beam in accordance with EN 1993-1-1 (2005). The shear connectors in this case were at 300 mm spacings, which exceeded the limits specified for the cross-section in Figure 1 according to Clause 6.6.5.5 of EN 1994-1-1 (2004), and hence EN 1993-1-1 (2005) was employed. The steel section was classified as Class 1.

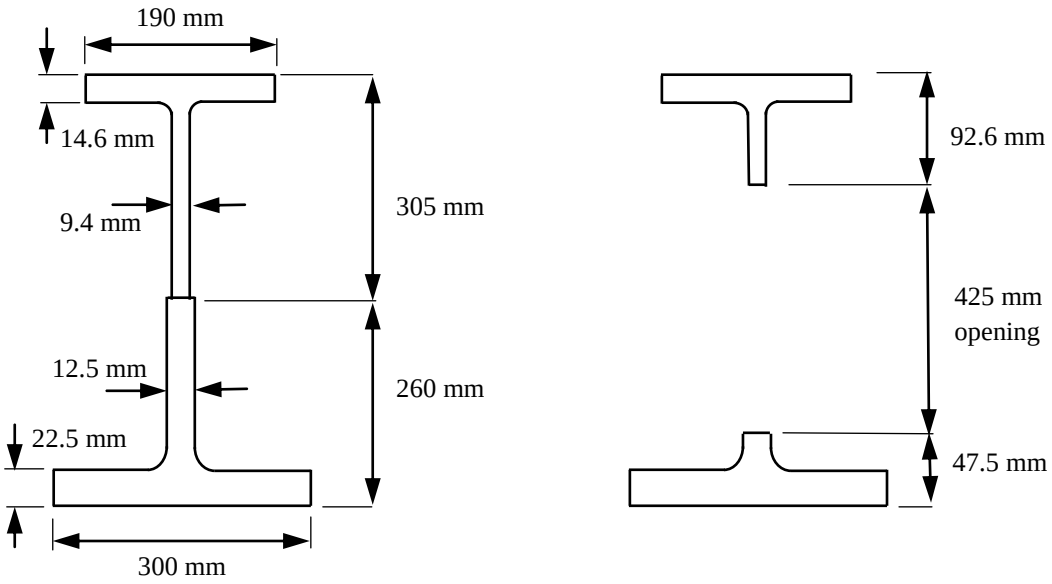

Figure 1 Cross-section dimensions of the asymmetric cellular beam

The elongated opening at the mid-span is 1105 mm long and was constructed by removing the central web-post. Some openings at or near to the load positions were fully or half in-filled to avoid local failure due to potential stress concentration and the arrangement of the openings was symmetrical about the mid-span. The steel deck profile was 80 mm deep and 0.9 mm thick with a 15 mm re-entrant stiffener on top. The deck rib spacing was 300 mm and a single 125 mm long × 19 mm diameter shear connector was placed in every rib, with 51 connectors in total. The welded height of the shear connectors was 120 mm. A193 mesh reinforcement (7 mm wire; 200 mm × 200 mm grid) was placed at the same level as the top of the welded shear connector. The concrete slab depth was 150 mm and thus the minimum concrete depth over the deck profile was only 55 mm and the concrete cover to the reinforcement was 30 mm. The concrete slab width was chosen as 3.0 m, primarily due to practical reasons and this would be less than the theoretical effective slab width for this beam span. Figure 2 (a) presents the steel cellular beam prior to placing the decking and Figure 2 (b) depicts the view of the top of the beam, with the shear studs welded into place.

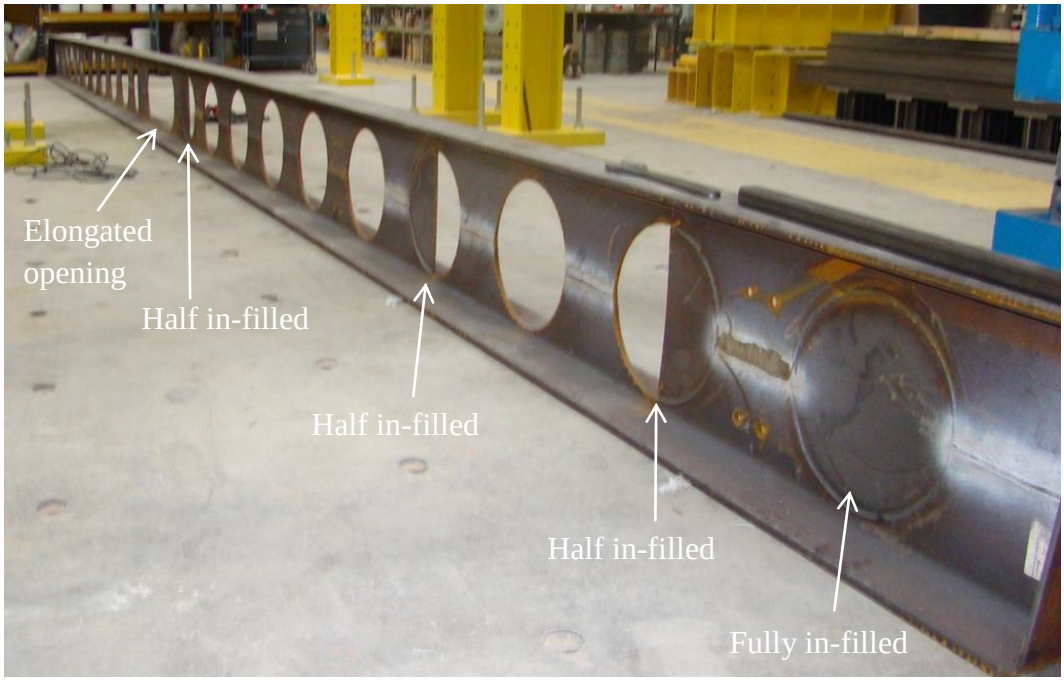

(a) prior to installing decking and shear studs

(b) after installation of profile decking and shear studs

Figure 2 Set up of the cellular steel beam

2.2 Specimen preparation

One of the aims of this project was to investigate the beam response using un-propped construction. A novel system was employed in order to achieve this. The arrangement is shown in Figure 3. IPE 200 sections were arranged like "wings" and bolted onto the web of the cellular beam at 6 locations along the length. Attached to the other end of these sections were IPE 200 sections running in the longitudinal direction. These supported the decking during concrete pouring and transferred the load through the wings back to the cellular beam. The "wing" system was removed after the concrete had gained its design strength.

Figure 3 "Wing" system used to support wet concrete slab weight

The cellular steel beam was delivered with a pre-camber of 40 mm (at the mid-span) which was achieved during the cutting and re-welding process. The measured vertical deflection at mid-span of the beam after concreting was 38 mm due to a concrete load of 2.7 kN/m^2. Therefore after concreting, the top surface of the composite beam was approximate level. The beam and decking weight was 0.5 kN/m^2, but the deflection of the beam due to these initial loads was not measured. No further deflection of the beam occurred once the "wing" support system was removed.

2.3 Material Properties

The steel grades of the top and bottom T-sections was S355 with a yield strength of 410 N/mm^2 (from mill certificates). The concrete compressive cube strength was about 30 MPa, obtained from material tests. The selected steel deck profile was grade S450 steel. Push out tests on the same deck profile showed that the mean value of the shear resistance of the shear connectors was about 70 kN.

3 Uniformly distributed load test

3.1 Test set-up

Two series of tests were carried out to the composite beam. In the first series, 8 point loads were applied to the beam to simulate a uniformly distributed load at the slab top surface. This was accomplished using 3 hydraulic actuators and a system of spreader beams as shown in Figure 4.

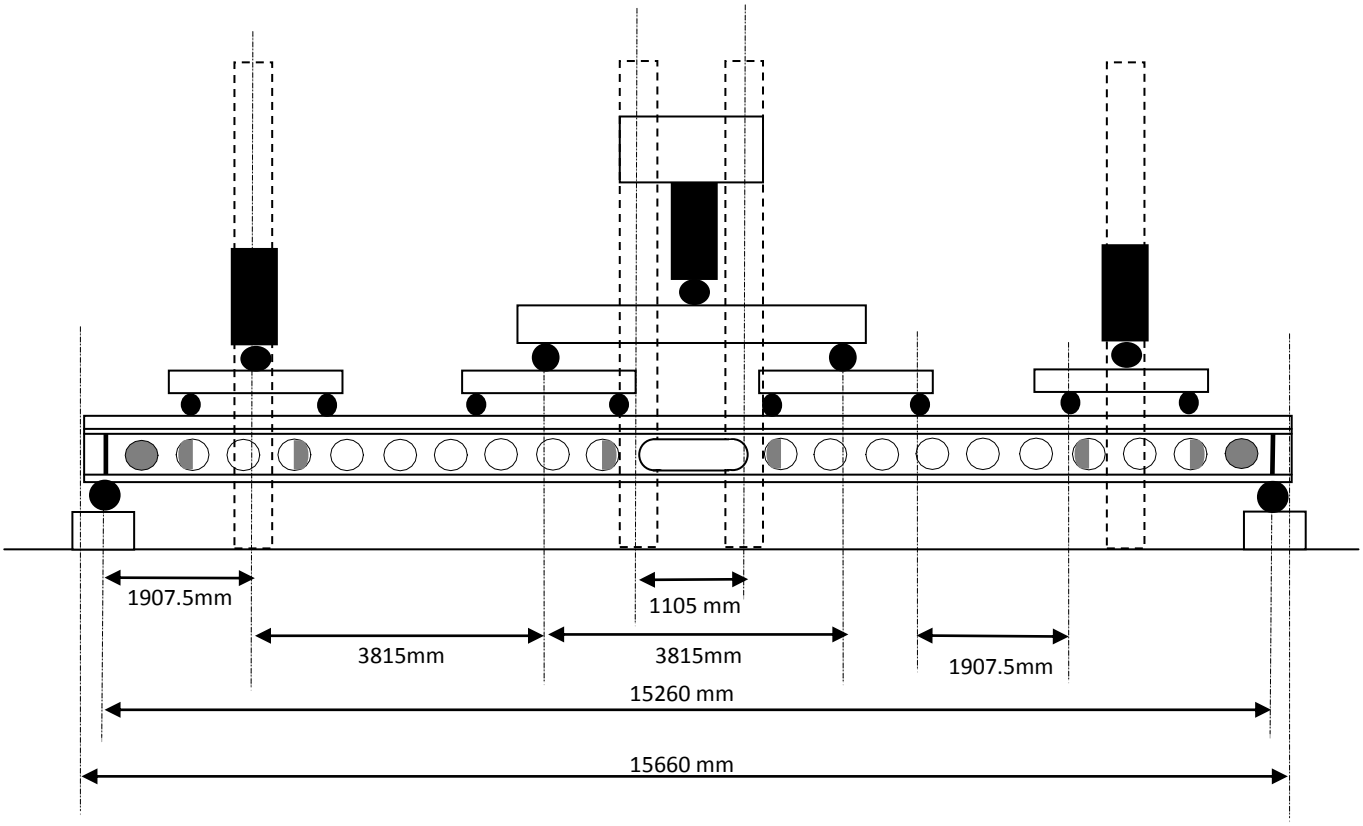

Figure 4 Set-up for uniformly distributed load test.

5 loading regimes were performed:

- Applied load up to 1.0 × working load (5 kN/m^2, or total load of 230 kN)
- Applied load up to 1.5 × working load (7.5 kN/m^2, or total load of 345 kN)
- Applied load up to 2.4 × working load (12 kN/m^2, or total load of 550 kN)
- Applied load up to failure (3.4 × working load: 17.2 kN/m^2, or total load of 785 kN)
- Repeat of applied failure load

The aforementioned load included the weight of the spreader beams but not the self-weight of the composite beam. The test was continued until a deflection of span/100 (153 mm) occurred at the mid-span, at which point it was considered that the failure was reached.

3.2 Instrumentation

The deformation and slippage of the beam were measured using 15 LVDTs. 9 of these recorded vertical displacements on the underside of the beam, 8 of which were located under the load application points as shown in Figure 5. The 5th vertical LVDT was located at mid-span. 2 LVDTs measured the slippage between the concrete slab and steel beam at the ends and the remaining 4 measured the slip between the steel deck and steel beam. 20 strain gauges were used to measure the longitudinal strain at different points on the web and flange of the steel beam and 4 strain gauges measured the longitudinal strain on the top face of the concrete slab at the mid-length. Figure 5 shows the positions of LVDTs along the beam length and the strain gauge numbering and arrangement at various cross-sections (S0, S1, S2, etc.) along the beam. LVDT-12, LVDT-13, LVDT-14 and LVDT-15 were omitted from the figure for the purposes of clarity. These remaining LVDTs measured the slip between the steel beam and decking with LVDT-12 and LVDT-15 located approximately 600 mm from the end supports (at the 3rd shear stud) and LVDT-13 and LVDT-14 at approximately 1800 mm from the supports (in the vicinity of the 7th shear stud).

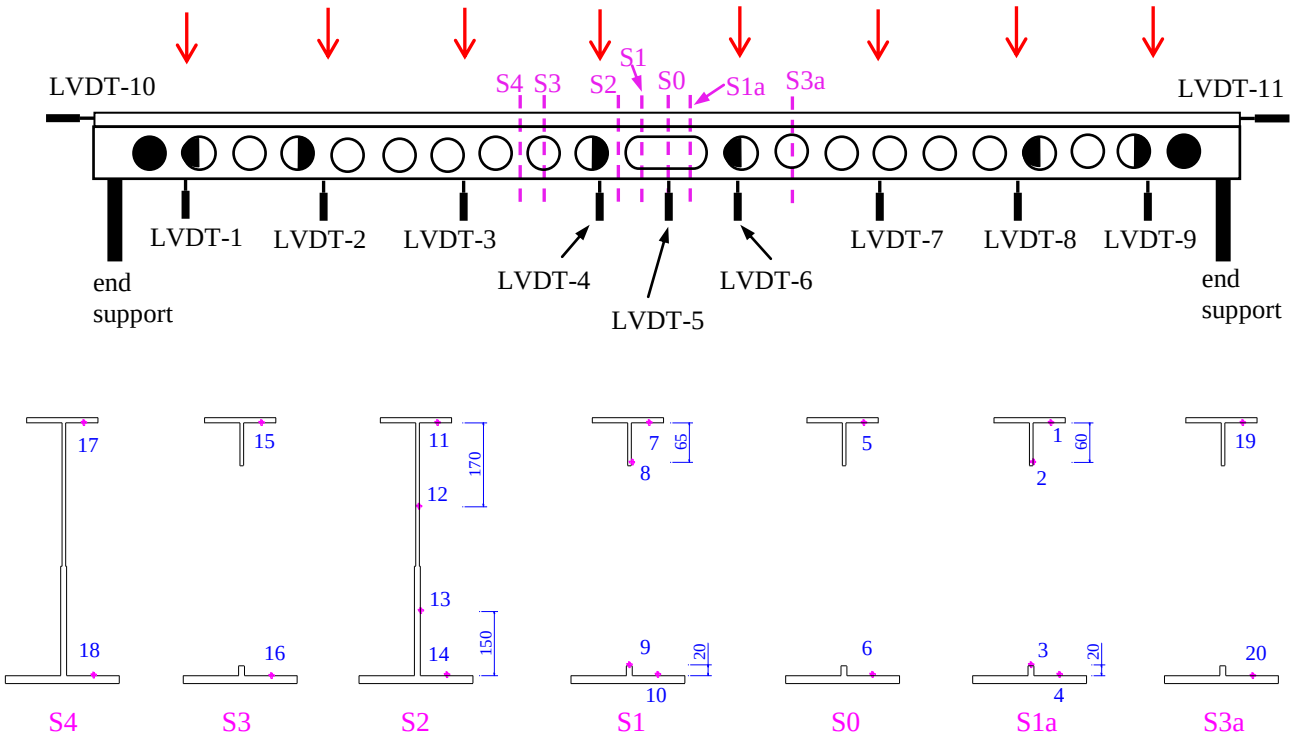

Figure 5 Location of instrumentation for uniformly distributed load test

3.3 Experimental results

3.3.1 Vertical deflection at beam mid-span

Steel beam mid-span deflections in the uniformly distributed load test are presented in Table 1.

Table 1 Deflection at mid-span (LVDT_5) observed in the uniformly distributed load test

Cycle	1.0 × working load	1.5 × working load	2.4 × working load	3.4 × working load (C1)	3.4 × working load (C2)
Load (kN/m^2)	5.0	7.5	12.0	17.2	16.7
Deflection at maximum load in individual cycle (mm)	22.8	35.2	65.3	142.6	118.0
Residual deflection at end of cycle (mm)	1.8	2.0	5.4	35.8	53.5
Cumulative residual deflection before this loading cycle (mm)	0	1.8	3.8	9.2	45
Cumulative deflection at maximum load (mm)	22.8	37.0	69.1	151.8	163.0

Residual deflection = deflection on unloading after each load cycle

The load-deflection relationship at the mid-span is presented in Figure 6. A residual deflection was observed in each cycle after unloading, which increased with progressive cycles. As stated previously, the test continued until the mid-span deflection reached $L/100$ (153 mm), at which point failure was deemed to have occurred. The failure load measured during the test was 17.2 kN/m^2 (imposed load). If the self-weight of the cellular beam (0.5 kN/m^2) and the concrete slab (2.7 kN/m^2) are taken into consideration, the total failure load is 20.4 kN/m^2. This represents a global factor of safety of 2.5 relative to the un-factored loading of 8.2 kN/m^2 (working load 5 kN/m^2 plus 0.5 kN/m^2 plus 2.7 kN/m^2). It was not possible to achieve this load during the last test in the series (3.4 × working load (C2)), since failure had already occurred, and this is reflected in the large value of cumulative deflection at the mid-span (163 mm). The load-deflection graph is approximately linear up to a load of 7.5 kN/m^2, and this is evidenced by the low residual deflection and degree of end slip upon un-loading.

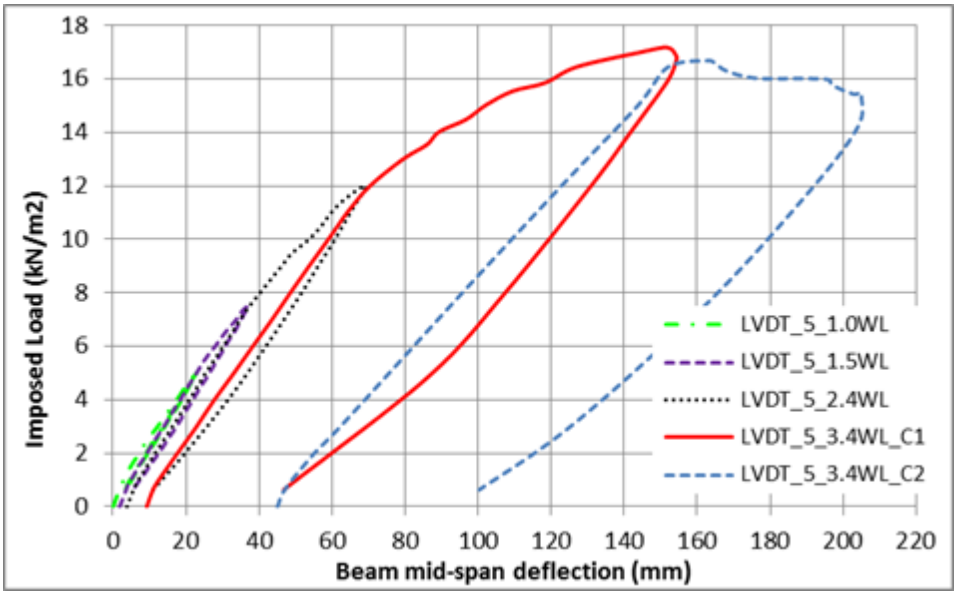

Figure 6 Relationship between applied load and mid-span deflection

3.3.2 Slip between slab and steel beam at ends

The end slips between steel beam and concrete slab at both ends of the composite beam (measured by LVDT_10 and LVDT_11) are presented in Table 2 and Figures 7 - 8. The slips were 13.5 mm and 8.5 mm at each end under the maximum applied load of 17.2 kN/m^2. According to Eurocode 4 Clause 6.6.1.1, shear connector behaviour is ductile if the connector can undergo a slippage of at least 6 mm,

which is considerably lower than the observed end slips. In Figures 7 – 8, nonlinearity in the load-slip curve occurred for loads exceeding 8 kN/m^2, over 1.5 working load or approximately half of the eventual failure load.

Table 2 End slip between slab and steel beam observed in the uniformly distributed load test

Cycle	1.0 × working load	1.5 × working load	2.4 × working load	3.4 × working load (C1)	3.4 × working load (C2)
Load (kN/m^2)	5.0	7.5	12.0	17.2	16.7
Slip at max. load by LVDT_10 in individual cycle (mm)	0.08	0.22	1.05	8.17	3.68
Residual slip by LVDT_10 in individual load cycle (mm)	0.01	0.03	0.31	5.01	0.48
Cumulative residual slip by LVDT_10 before this load cycle (mm)	0.0	0.01	0.04	0.35	5.36
Cumulative slip by LVDT_10 at max. load (mm)	0.08	0.23	1.09	8.52	9.04
Slip at max. load by LVDT_11 in individual load cycle (mm)	0.08	0.24	2.37	12.68	14.58
Residual slip by LVDT_11 in individual load cycle (mm)	0.01	0.04	0.83	7.64	9.80
Cumulative residual slip by LVDT_11 before this load cycle (mm)	0.0	0.01	0.05	0.88	8.52
Cumulative slip by LVDT_11 at max. load (mm)	0.08	0.25	2.42	13.56	23.10

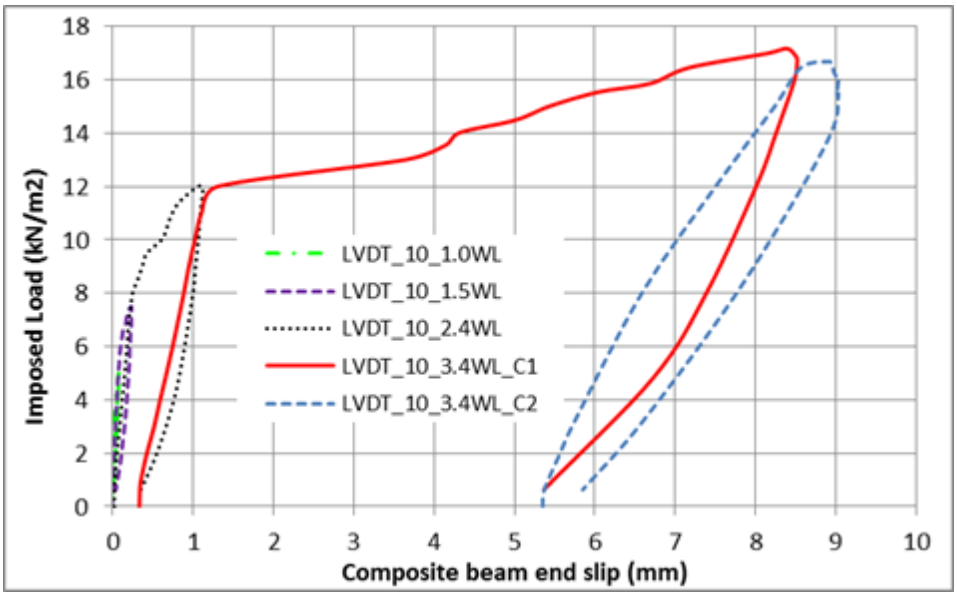

Figure 7 Relationship between applied load and end-slip measured by LVDT_10

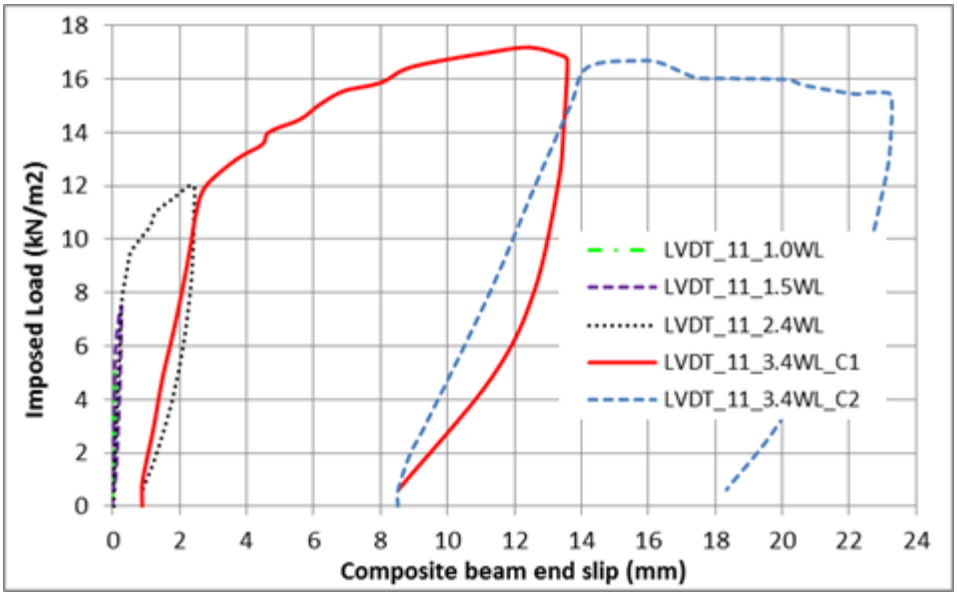

Figure 8 Relationship between applied load and end-slip measured by LVDT_11

3.3.3 Typical strains measured at steel beam and concrete slab

The strains measured in the steel beam and concrete slab are presented in Table 3. A strain of 1950με ($\mu\varepsilon=10^{-6}$ or micro-strain) is equivalent to the yield strength of the steel of 410 N/mm^2. At the maximum load, the compression strain in the top flange (measured by strain gauge S_1) was 1065με, and the tensile strain in the bottom (S_20) flange was 1995με, which indicated that the bottom flange had reached its yield resistance. If one takes into consideration the residual strains in the previous test cycles, the compression strain in the top flange and tensile strain in the bottom flange were 1205με and 2295με respectively.

The typical strain in the concrete (measured by strain gauge SC_2) at the maximum applied load of 17.2 kN/m^2 was 865με (0.086%), which is less than the maximum strain of 0.2% (2000 με) that is experienced by concrete at its maximum strength. For an elastic modulus of 32000 MPa the measured strain is theoretically equivalent to a compressive stress of 27.7 N/mm^2 in the concrete although the actual stress will be less because of the non-linear stress-strain curve for concrete.

Table 3 Measured strains (με) in the steel flanges and the top surface of the concrete slab

Cycle	1.0 × working load	1.5 × working load	2.4 × working load	3.4 × working load (C1)	3.4 × working load (C2)
Load (kN/m^2)	5.0	7.5	12.0	17.2	16.7
(S_1) at max. load in this load cycle	-70	-110	-250	-1065	-700 *
Residual (S_1) after this cycle	-30	-30	-80	-485	-310
Cumulative residual strain (S_1) before this load cycle	0	-30	-60	-140	-625
Cumulative strain (S_1) at max. load	-70	-140	-310	-1205	-1325 **
(S_20) at max. load in this load cycle	470	700	1190	1995	1630
Residual (S_20) after this cycle	80	80	140	425	-50
Cumulative residual strain (S_20) before this load cycle	0	80	160	300	730
Cumulative strain (S_20) at max. load	470	780	1350	2295	2360
(SC_2) at max. load in this cycle	-240	-350	-600	-865	810
Residual (SC_2) after this cycle	-50	-50	-70	-45	-60
Cumulative residual (SC_2) before this load cycle	0	-50	-100	-170	-215
Cumulative (SC_2) at max. load	-240	-400	-700	-1035	-1025

μ = 10–6 or micro strain

* Reached maximum value (-1070) later in the test when the imposed load dropped down to 14.3MPa

** Reached maximum value (-1690) later in the test when the imposed load dropped down to 14.3MPa

Figure s 9 to 11 present the typical measured strains in the bottom flange, top flange and top surface of the concrete slab at the mid-span. Non linearity occurred at an equivalent uniform load of about 12 kN/m^2 or 70% of the failure load 17.2 kN/m^2. The concrete strain is approximately linear up to failure.

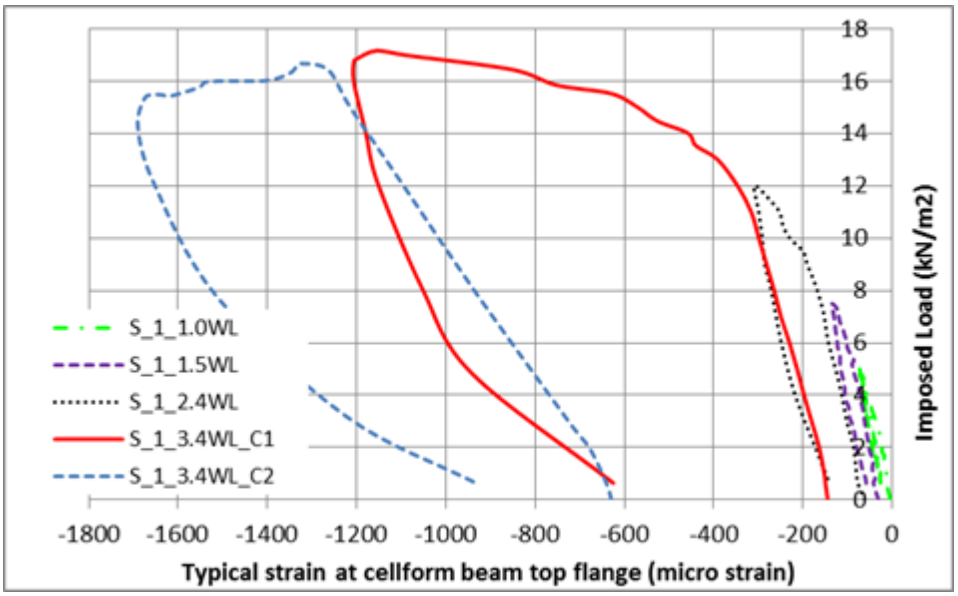

Figure 9 Relationship between applied load and strain in top flange at mid-length

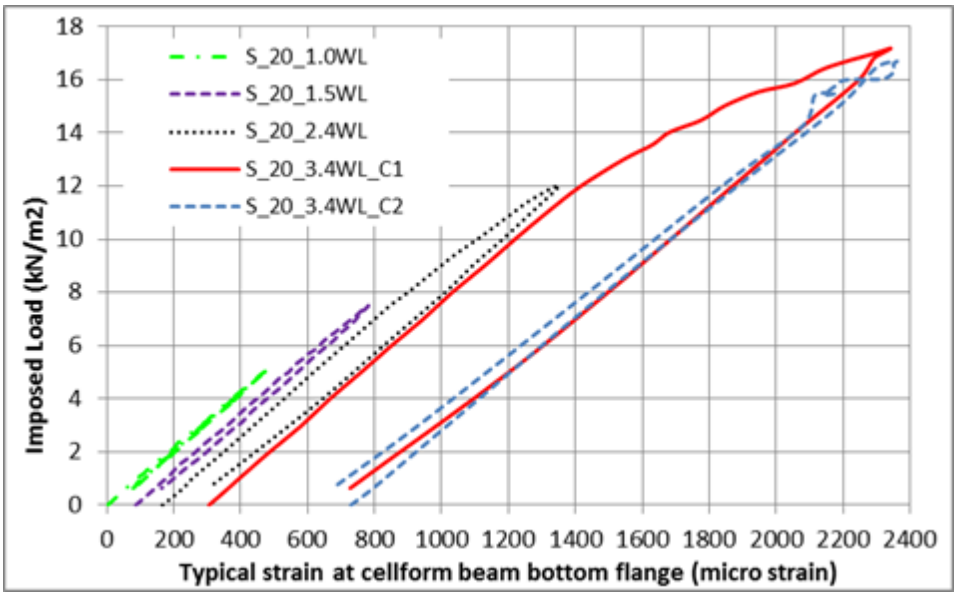

Figure 10 Relationship between applied load and strain in bottom flange at mid-length

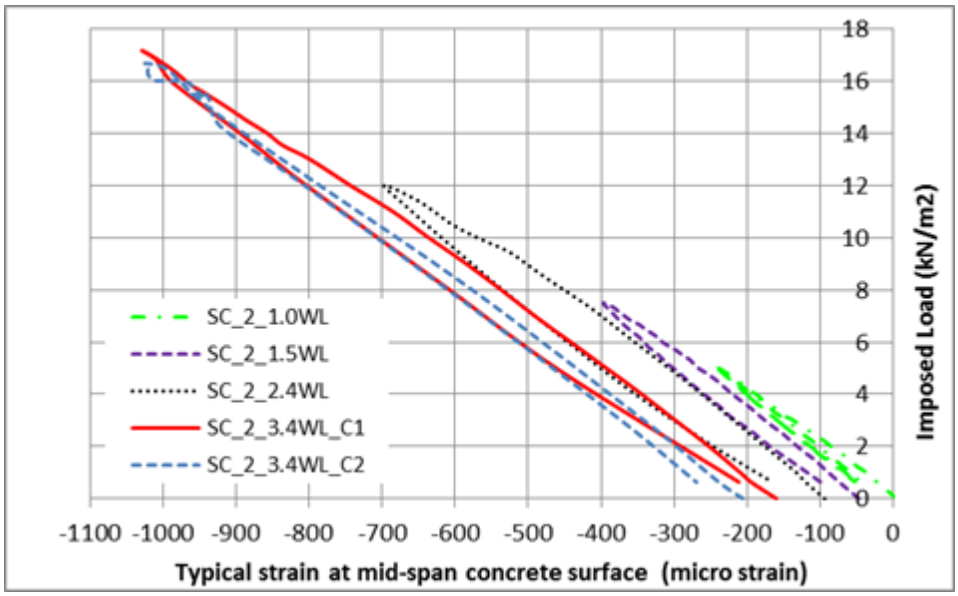

Figure 11 Relationship between applied load and strain in top surface of concrete slab at mid-length

The strains that occurred in the steel beam during concrete pouring are presented in Table 4. The self-weight of the concrete was estimated to be 2.7 kN/m^2. The maximum tensile strain at the bottom flange is about 270 με and maximum compressive strain at the top flange is about 500 με. These values are all considerably lower than 2000 με. The strain monitoring place ID is shown in Figure 5 as the strain gauge numbering.

Table 4 Typical strains (με) of steel beam caused by wet concrete weight

Monitoring Place ID	1	2	3	4	5	6	7	8
Before Concreting	0	0	0	0	0	0	0	0
After Concreting	-502	-587	254	277	-497	260	-477	-653
Monitoring Place ID	9	10	11	12	13	14	15	16
Before Concreting	0	0	0	0	0	0	0	0
After Concreting	340	269	-475	-79	22	247	-517	266

3.3.4 Strain distribution along beam axis and at different beam sections

Table 5 shows the strain distribution in the top and bottom flanges along the beam axis. It can be seen that the maximum tensile strain occurred at a distance from the end support of 5930 mm, not at the mid-span (distance to end support of 7630 mm). Table 6 shows the strain distribution in different monitoring sections. Very high strains occurred at the web of the elongated opening (point 9 at section S1 and point 3 at section S1a). These were higher than the strains in the flange and the only possible explanation is that twisting occurred.

Table 5 Measured strains in the steel beam at the maximum imposed load 17.2 kN/m^2

Top flange				Bottom flange			
Monitoring position point ID	Distance from support end (mm)	Strain with previous residual strain	Strain without previous residual	Monitoring position point ID	Distance from support end (mm)	Strain with previous residual strain	Strain without previous residual
17	5590	-970	-840	18	5590	1563	1378
15	5930	-960	-830	16	5930	2220	1882
11	6950	-754	-637	14	6950	1691	1490
7	7290	-730	-628	10	7290	2119	1850
5	7630	-860	-756	6	7630	1799	1610
1	7290	-1150	-1015	4	7290	2140	1823
19	5930	-	-	20	5930	2340	2039

Table 6 Measured strains in different sections at the maximum imposed load 17.2 kN/m^2

Section position ID	Monitoring point position ID	Distance to bottom flange (mm)	Monitoring point position	Strain with previous residual	Strain without previous residual
S0	5	528	top flange	-859	-755
	6	0	bottom flange	1799	1610
S1	7	528	top flange	-730	-628
	8	463	web	-660	-562
	9	20	web	4497	3691
	10	0	bottom flange	2119	1850
S2	11	528	top flange	-754	-637
	12	358	web	-154	-159
	13	150	web	90	56
	14	0	bottom flange	1690	1490
S3	15	528	top flange	-958	-831
	16	0	bottom flange	2220	1882
S4	17	528	top flange	-971	-846
	18	0	bottom flange	1564	1378
S1a	1	528	top flange	-1155	-16
	2	468	web	-712	-570
	3	20	web	5195	3918
	4	0	bottom flange	2140	1283
S3a	19	528	top flange	-	-
	20	0	bottom flange	2340	2039

4 Shear load test

4.1 Test set-up

In the second series of tests, point loads were applied at 5/16 and 7/16 of the span, resulting in a shear force across the elongated opening. The testing arrangement is shown in Figure 12.

4 tests were performed:

- Applied load up to 108kN
- Applied load up to 169kN
- Applied load up to 388kN
- Applied load up to 405kN

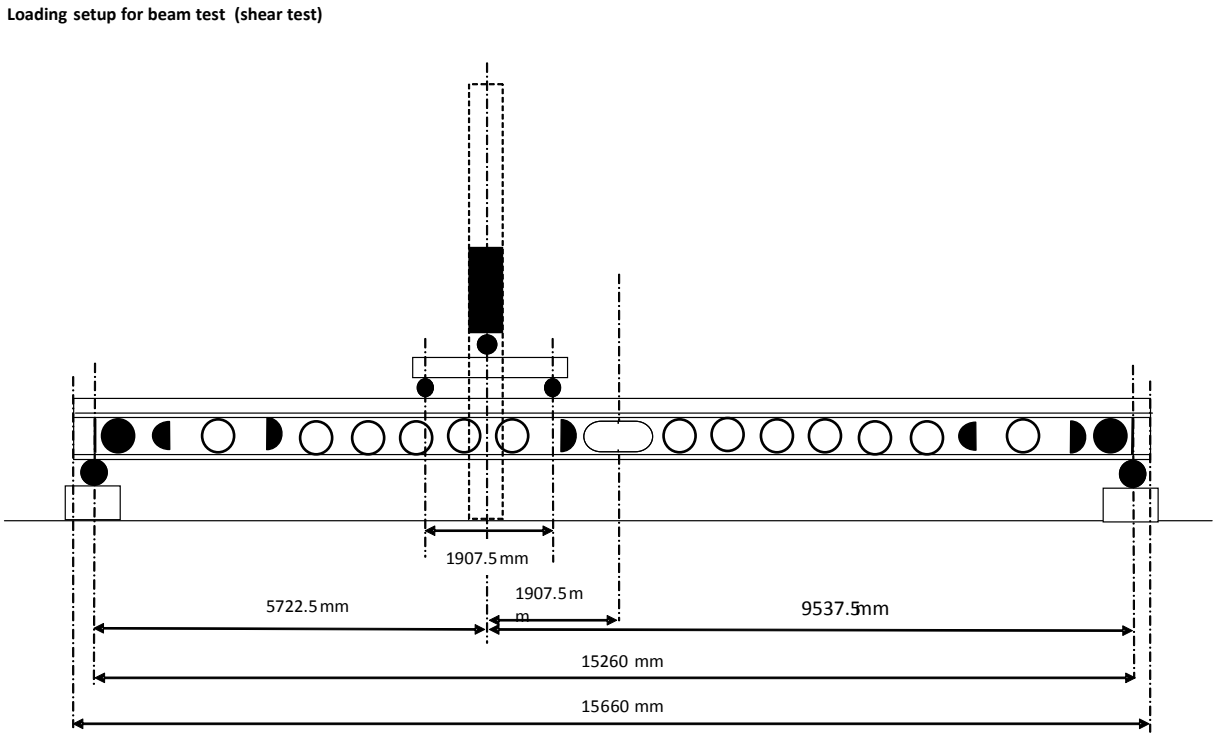

Figure 12 Testing arrangement for shear load test

4.2 Monitoring positions and instrumentation

In this series of tests, it was assumed that the shear connection at the mid span had not been affected by the uniformly distributed loading from the previous test series and so the Vierendeel bending resistance due to composite action would not be reduced due to the first test. The same strain gauge configuration was used as in the first test (see Figure 5). 15 LVDTs were used to measure displacements at different locations. The positions of LVDTs 1-11 are shown in Figure 13 with LVDTs 1-9 measuring vertical deflection on the underside of the steel beam and LVDTs 10 and 11 measuring the end-slip. LVDTs 12 and 15 measured the slip between the steel decking and steel beam at approximately 600 mm from the end supports while LVDTs 13 and 14 measured the separation between top flange of the steel beam and the steel decking at the edges of the elongated opening, directly above LVDTs 3 and 7.

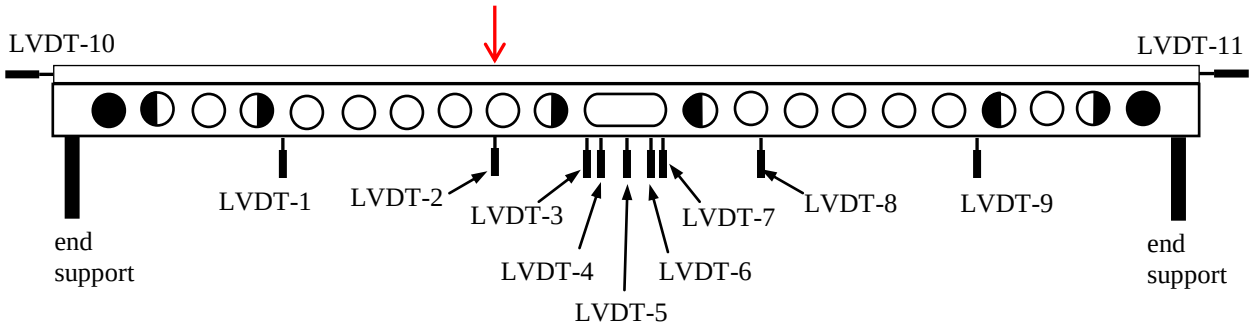

Figure 13 Positions of LVDTs for shear load test

4.3 Experimental results

4.3.1 Beam deflections

Figures 14 and 15 show the load versus deflection relationships at the loading positions and the beam mid-span. In a similar manner to the uniformly distributed load test series, a residual deflection was observed at the end of each loading cycle, which increased in subsequent cycles. The failure load (maximum applied load) was 405 kN. This load includes the weight of the spreader beams but does not include the self-weight of the concrete slab. The figures show that the non-linearity in the load-deflection curve only occurred at a load over 300 kN, or about 75% of the failure load.

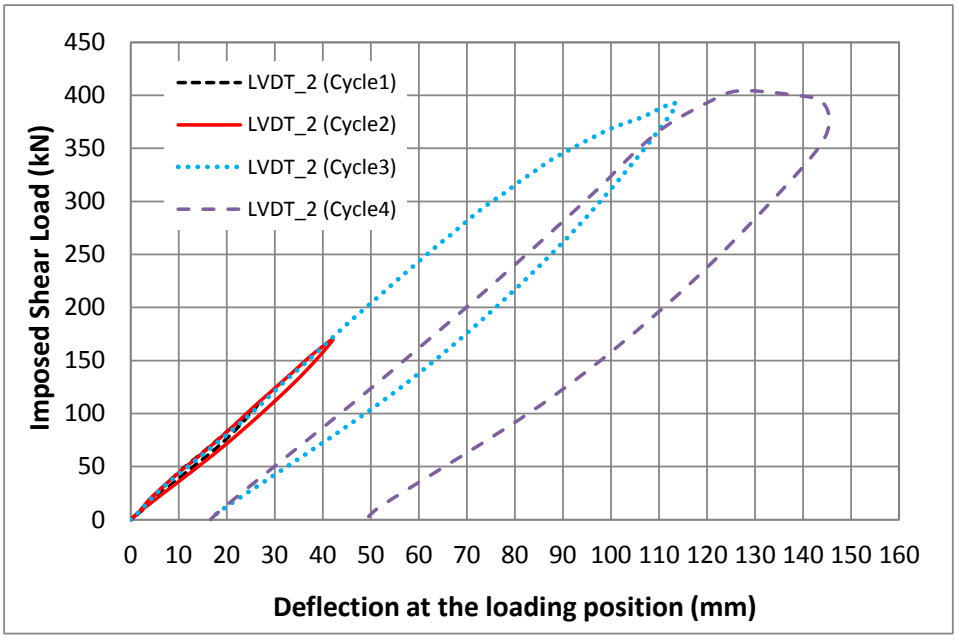

Figure 14 Applied load versus deflection at loading position

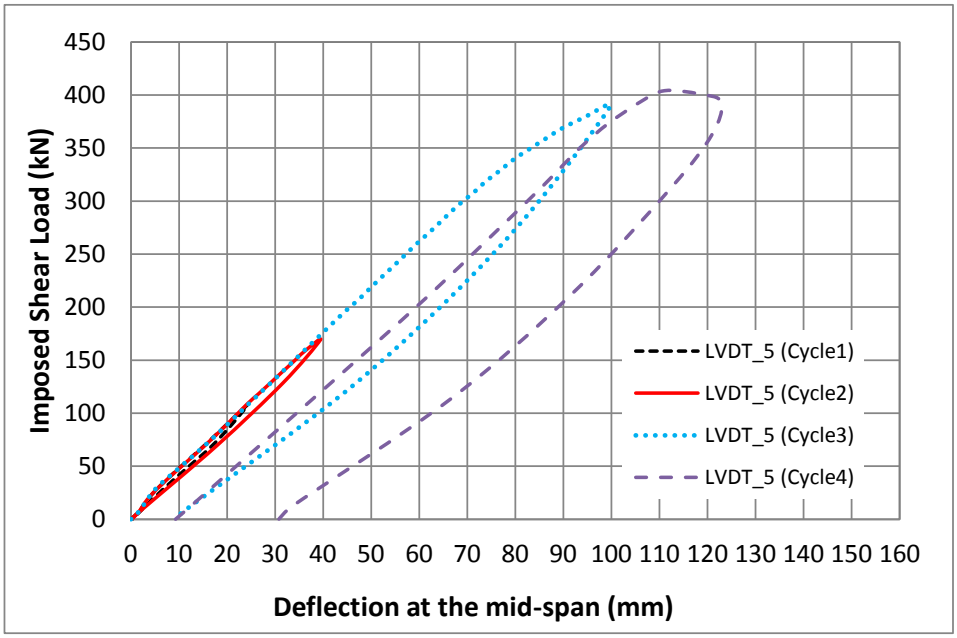

Figure 15 Applied load versus deflection at mid-span

The vertical deflections measured along the beam from LVDTs 2-7 in Cycles 1-4 are presented in Table 7. The deflection at the maximum load and the residual deflection are given in each case. The largest vertical deflections were 127.0 mm, measured by LVDTs 3 and 4 and 126.4 mm, measured by LVDT_2 during Cycle-4. These were the 3 LVDTS that were closest to the applied shear load. The smallest vertical deflection from Cycle-4 in Table 8 is 88.9 mm, recorded by LVDT_7, which was at the opposite end of the beam to LVDTs 2-4. These values reflect the asymmetry of the deflected shape under shear load.

Table 7 Deflection recorded by LVDTs_2, 3, 4, 5, 6 and 7

Cycle number		Cycle-1	Cycle-2	Cycle-3	Cycle-4
Maximum load		107.7kN	168.9kN	387.8kN	404.1kN
LVDT_2	Cumulative deflection at maximum load	26.4	42.0	113.3*	126.4
	Cumulative residual deflection	0.26	0.05	16.6	48.9
LVDT_3	Cumulative deflection at maximum load	21.3	36.7	112.1	127.0
	Cumulative residual deflection after this cycle	0.05	0.05	15.2	53.5
LVDT_4	Cumulative deflection at maximum load	25.5	41.1	113.4	127.0
	Cumulative residual deflection after this cycle	0.31	0.35	17.7	57.2
LVDT_5	Cumulative deflection at maximum load	24.3	39.4	99.6	111.1
	Cumulative residual deflection after this cycle	0.25	0.21	9.3	30.8
LVDT_6	Cumulative deflection at maximum load	22.8	36.8	83.9	91.9
	Cumulative residual deflection after this cycle	0.19	0.07	0.01	8.6
LVDT_7	Cumulative deflection at maximum load	22.6	36.5	81.8	88.9
	Cumulative residual deflection after this cycle	0.14	0.04	-1.0	3.8
Relative deflection around the elongated opening at maximum applied loads		LVDT_5 – LVDT_7		17.8	22.2
		LVDT_3 – LVDT_5		12.5	15.9
		LVDT_5 – LVDT_6		15.7	19.2
		LVDT_4 – LVDT_5		13.8	15.9

* This value is calculated by comparing with other monitoring data due to the LVDT reaching its maximum travel at 103.6mm. The deflection in Cycle-4 showed in the table included the residual deflection of Cycle-3 (please view the figures 14 and 15). From the figures, it can be seen that the deflection after the maximum load shows a good degree of ductility around the maximum load

The relative deflections between the two ends of the elongated opening are shown in Figures 16 and 17. Figure 16 covers the section of beam from LVDT 3-7 whereas Figure 17 focusses on a smaller region of the beam around the opening, from LVDTs 4-6. The relative deflection due to Vierendeel bending was approximately 30 mm at the maximum load.

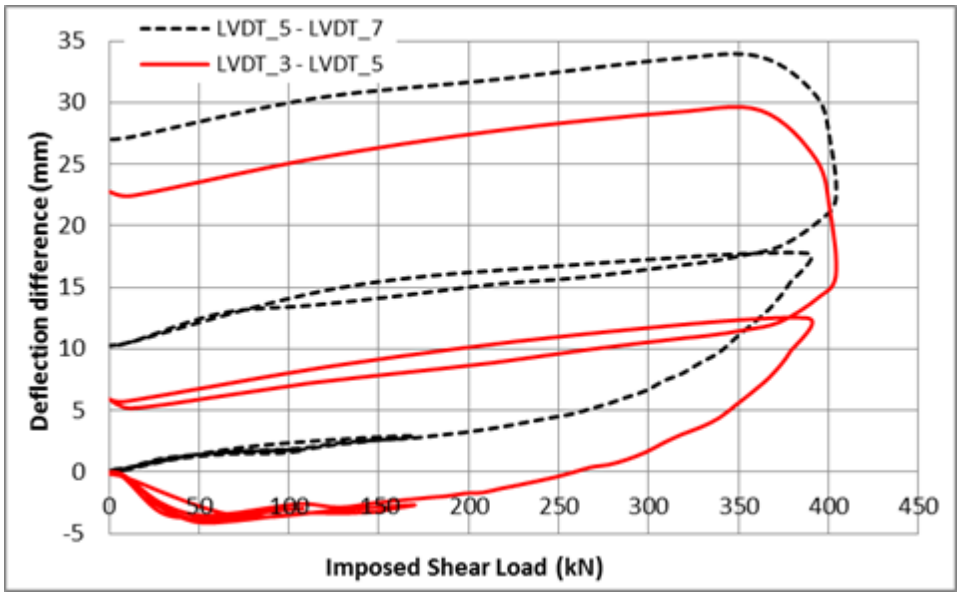

Figure 16 Load versus deflection difference from LVDT_3 to LVDT_7

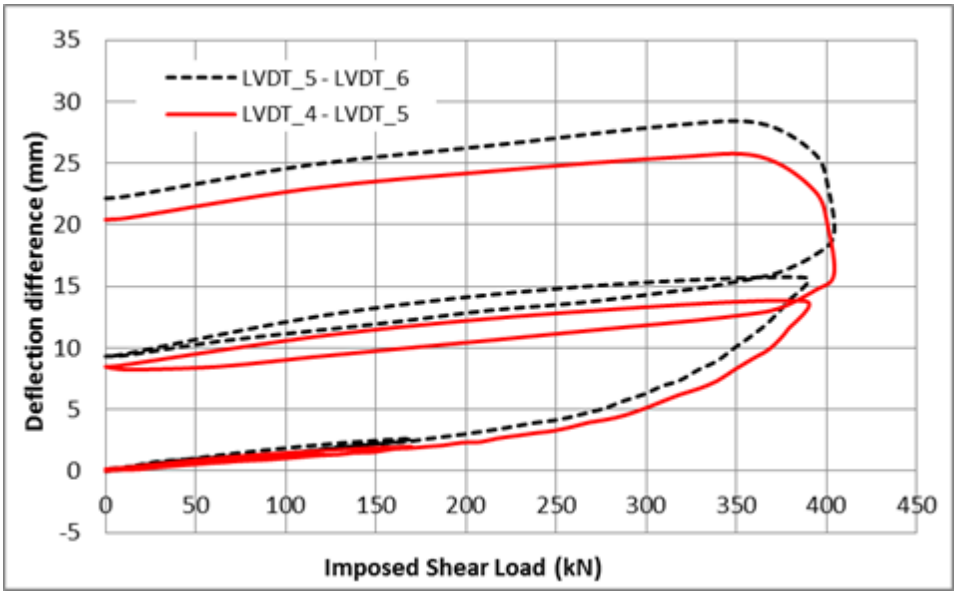

Figure 17 Load versus deflection difference from LVDT_4 to LVDT_6

The deflected shape of the composite beam at the end of the shear load test is shown in Figure 18, in which the Vierendeel failure mode is apparent in the steel section.

Figure 18 Deflected shape of the beam and elongated opening

4.4 End-slip

Table 8 shows the accumulated end slip at maximum load and residual slip in each loading cycle, measured by LVDTs 10 and 11.

Figure 19 and 20 show the load versus end slip relationships. In the final cycle little residual end slip was observed in the measurements of LVDT_10. However larger end-slips and notable residual end-slips were detected by LVDT_11 as shown in Figure 20.

Table 8 Slip between slab and steel beam recorded by LVDTs_10, 11 (LVDT_10 is at the load side):

Cycle number		Cycle-1	Cycle-2	Cycle-3	Cycle-4
Maximum load (kN)		108	169	388	405
LVDT_10	Cumulative slip at maximum load (mm)	0.56	0.86	2.65	4.2
	Cumulative residual slip after this cycle (mm)	0.01	0	0.08	0.2
LVDT_11	Cumulative slip at maximum load (mm)	0.75	1.29	4.29	7.3
	Cumulative residual slip after this cycle (mm)	0.03	0.02	0.87	4.8

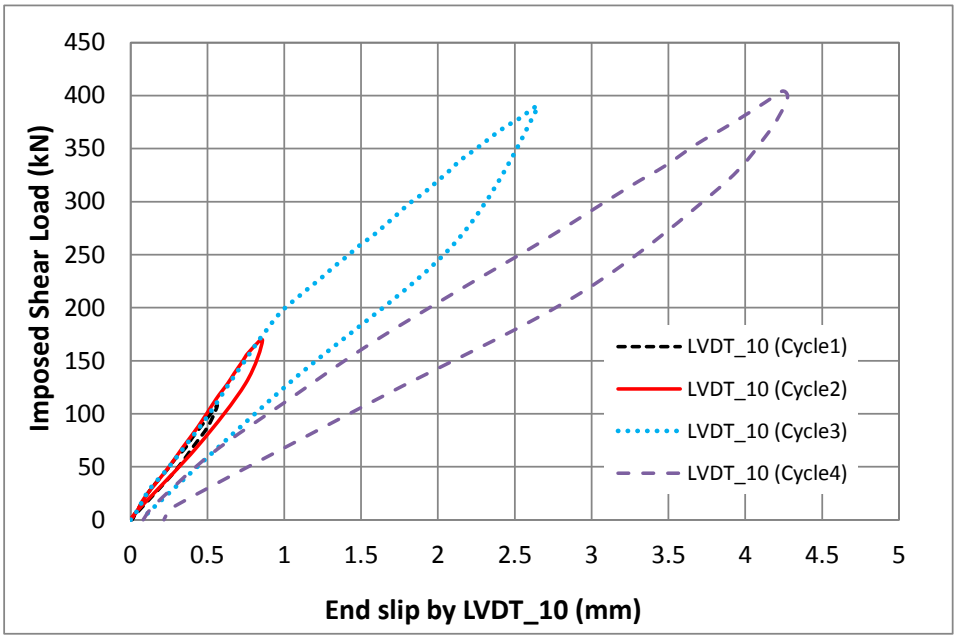

Figure 19 Applied load versus end slip measured by LVDT_10

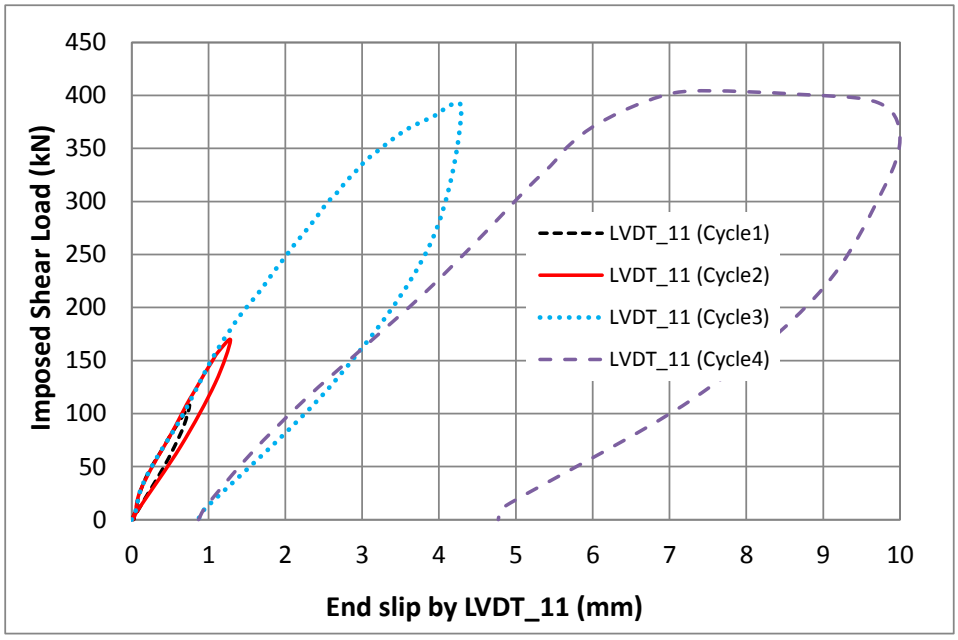

Figure 20 Applied load versus end slip measured by LVDT_11

4.5 Strain distribution

Tables 9 and 10 present the strains measured at various monitoring points in the steel beam close to the mid-span, using the numbering system outlined in Figure 5. The largest tensile strain occurred at Point 11 in the top flange, 6950 mm from the end support, in a section of the beam without web openings adjacent to the elongated opening. The largest compressive strain was at Point 1, 7290 mm from the end support, in the top flange of the elongated opening. Point 11 was the only monitoring point in the top flange that was in tension. This point was close to the loading point at 7/16 of the span. In other monitored areas of the beam, the top flange was in compression while the bottom was in tension. Points 3 and 9 were located in the web of the bottom Tee in the elongated opening. Strains in both of these were compressive despite the tensile strains in points 4, 6 and 10 in the bottom flange. It is also worth noting the tensile strain in point 8, in the web of the top Tee in the elongated opening. Points 1, 5 and 7 in the top flange at the opening were in compression. It appears from these strain patterns that each Tee-section at the elongated opening was acting independently in bending. This was distinct from the uniformly distributed load case, where the entire bottom Tee was in tension and entire top Tee was in compression. The visible twisting that occurred under the previous load case was not observed under the applied shear load.

Table 9 Summary of measured strains in the steel beam at the maximum shear load by monitoring locations

Top flange				Bottom flange			
Monitoring position point ID	Distance from support end (mm)	Strain with previous residual strain	Strain without previous residual	Monitoring position point ID	Distance from support end (mm)	Strain with previous residual strain	Strain without previous residual
17	5590	-4453	-941	18	5590	191	816
15	5930	-4134	-604	16	5930	-	-
11	6950	4912	3060	14	6950	1083	1238
7	7290	-783	-860	10	7290	1253	1241
5	7630	-262	-176	6	7630	1314	1256
1	7290	-5871	-1577	4	7290	-57	-14
19	5930	-714	-800	20	5930	1124	1111

Table 10 Summary of measured strains in the steel beam at the maximum shear load by monitored beam sections

Section position ID	Monitoring point position ID	Distance to bot flange (mm)	Monitoring point position	Strain with previous residual	Strain without previous residual
S0	5	528	top flange	-262	-176
	6	0	bottom flange	1314	1256
S1	7	528	top flange	-783	-860
	8	463	web	1468	1463
	9	20	web	-802	-855
	10	0	bottom flange	1253	1241
S2	11	528	top flange	4912	3060
	12	358	web	3559	2216
	13	150	web	-873	-939
	14	0	bottom flange	1083	1238
S3	15	528	top flange	-4134	-604
	16	0	bottom flange	-	-
S4	17	528	top flange	-4453	-941
	18	0	bottom flange	191	816
S1a	1	528	top flange	-5871	-1577
	2	468	web	-3618	-169
	3	20	web	-725	-890
	4	0	bottom flange	57	-14
S3a	19	528	top flange	-714	-800
	20	0	bottom flange	1124	1111

5 Mode of Failure

During the uniformly distributed load test, failure was defined as a vertical deflection exceeding 1/100 of the beam span. After achieving this deflection, the specimen underwent a second cycle but failed to achieve the same maximum load of 17.2 kN/m^2. A very large cumulative end slip (23.1 mm) was observed at one end of the beam. The steel in the bottom flange at the mid-span had reached yield but was considerably below the ultimate strain, and the strains measured in the concrete slab at the mid-span were also lower than the value (2000 με) corresponding to the maximum compressive strength. Hence, under a uniformly distributed load, the beam had surpassed the serviceability limits in terms of deflection and the maximum load carrying capacity in bending. No shear stud failure was observed

and while parts of the steel beam had yielded, several of the strains in the monitoring regions were still in the elastic range.

For the shear load test, a plateau was observed in the load-deflection relationship indicating that the maximum load had been reached. Large deformations were observed in the Vierendeel mechanism and several regions of the steel beam had reached strains that were more than double the yield strain. To check the failure modes of the tested composite cellular beam, the concrete slab was cut alongside the vicinity of the longitudinal middle section after the shear load test. Horizontal shearing cracks inside the concrete, at the rib height, can be seen clearly from Figure 21.

Figure 21 Failure mode of concrete slab

The labels C2, C4… C22 are the circular cell's position. There are 22 cells (including the fully filled and half-filled cells), i.e., C22 is at one end of the beam. There was no horizontal crack inside the slab just above C7, C8 and C9. The concrete above C10 to C12, at the mid-span, was crushed inside. No shear connector failed under distributed load and shear load. Hence failure occurred by yielding of the steel beam followed by crushing of the concrete.

6 Analysis and Discussion

6.1 Shear stud capacity and degree of Shear Connection

The shear stud capacity was found to be approximately 70 kN from previous push-out tests. For a uniformly distributed load w, the bending moment at the mid-span of a beam of length L is $wL^2/8$ and hence the bending that occurred under maximum load of 20.4 kN/m^2 (including beam self-weight) on a 3.0 m wide slab was equal to 1790 kNm ($20.4\times3.0\times15.3^2/8$). Assuming a plastic stress distribution for the steel and concrete, and using the measured steel yield stress of 410 N/mm^2, the shear studs were found to have a capacity of 68.2 kN which was close to the 70 kN value obtained in push-out tests. Using this value for shear stud resistance, the degree of shear connection, η, was calculated by:

$$\eta = n/n_f \quad (1)$$

where n_f was the number of connectors for full shear connection

and n was the number of connectors provided.

η was calculated to be 36% using the shear stud capacity of 68.2 kN

In Eurocode 4, the minimum required degree of shear connection depends on the bottom flange area/top flange area ratio, the material strength and the member length. For steel sections with equal flanges, used as simply support beams with a span not exceeding 25 m, the degree of shear connection is calculated by

$$\eta \geq 1 - \left(\frac{355}{f_y}\right)(0.75 - 0.03L_e)\ ,\ \eta \geq 0.4 \quad (2)$$

For steel sections with a bottom flange area to top flange area ratio of 3, used as simply support beams with a span not exceeding 20 m, the degree of shear connection is calculated by

$$\eta \geq 1 - \left(\frac{355}{f_y}\right)(0.30 - 0.015L_e),\ \eta \geq 0.4 \quad (3)$$

as stated by Clause 6.6.1.2 in Eurocode 4. L_e is the span (or distance between points of zero bending) and f_y is the steel yield strength. According to this clause, η must not be below 40%. Lawson and Saverirajan [8] recognised that a lower degree of shear connection may be permissible in beams using unpropped construction and recommended using a reduction factor of $(M/M_{pl})^{1.5}$ for the minimum degree of shear connection in these cases, where M is the applied bending moment. Lawson and Saverirajan [8] also recommended keeping the degree of shear connection above 40%. The required degree of shear connection according to the Eurocode 4 guidelines was calculated to be 88% for this particular beam. Hence the actual degree of shear connection was considerably below this and even below the minimum of 40 %. If pairs of shear connectors had been used instead of single shear connectors, the degree of shear connection would have been 53%, which is still significantly lower than the 88% required by Eurocode 4.

6.2 Strain distribution

As discussed in Section 3.3.3, the strains in the steel beam were measured during the casting of the concrete. The strain in the top flange at the mid-length was 497με and the strain in the bottom flange was 260με. If one adds these strain values to the total accumulated strains during the uniformly distributed load test presented in Table 3, the strains in the top and bottom flanges increase from 1205με and 2295με to 1702με and 2555με respectively.

The position of the neutral axis can be estimated using values of strain in the top and bottom flanges of the beam and this is illustrated diagrammatically in Figure 22.

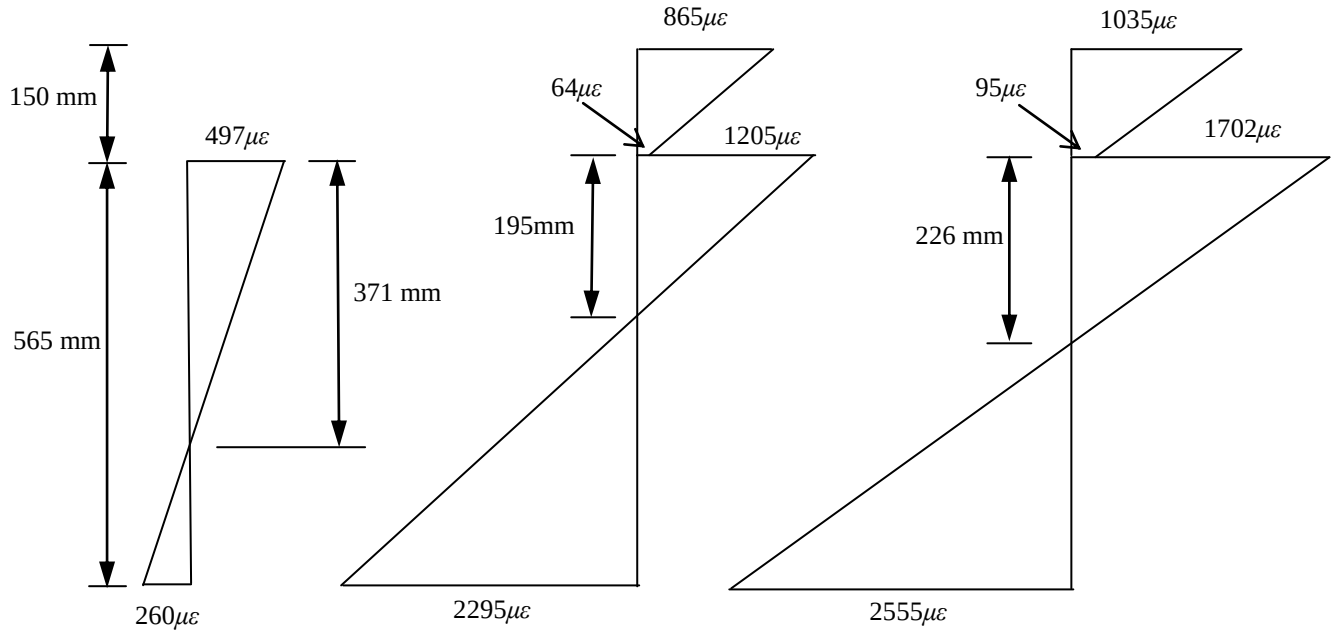

Figure 22 Strain distribution through cross-section depth corresponding to measured strains

As is seen in Figure 22, the depth of the neutral axis is 371 mm from the top of the steel beam after the pouring of the wet concrete. Under the maximum test load and only using the accumulated strains of 1205με and 2295με, the neutral axis depth during the test is estimated to be 195 mm. However, when the strains from the weight of the concrete are also included, the position of the neutral axis is lowered to 226 mm below the top of the beam. Similar approaches were used to estimate the position of the neutral axis for the lower loading cycles. The results are presented in Table 11 for each cycle, using the accumulated total strain from loading cycles. When the strains from the concrete self-weight are taken into account, the neutral axis appears to move upwards as the load increases up to the maximum load, and then moves downwards for the second cycle at 3.4 × working load, indicating that either the concrete or composite connection has failed at this stage.

Table 11 Estimated neutral axis position from strain measurements for each cycle under uniformly distributed load

Without residual strain from concrete pour		Considering residual strain from concrete pour	
Load	Neutral axis depth from top of steel beam	Load	Neutral axis depth from top of steel beam
1.0 × working load	73 mm	1.0 × working load	247 mm
1.5 × working load	86 mm	1.5 × working load	215 mm
2.4 × working load	106 mm	2.4 × working load	187 mm
3.4 × working load	195 mm	3.4 × working load	226 mm

The position of the elastic neutral axis of the steel beam, y_e is calculated as follows:

$$y_e = \frac{A_{bTf}\, y_{bTf} + A_{bTw} y_{bTw} + A_{tTf}\, y_{tTf} + A_{tTw} y_{tTw}}{A_{bTf} + A_{bTw} + A_{tTf} + A_{tTw}} \quad (4)$$

where A_{bTf}, A_{bTw}, A_{tTf} and A_{tTw} refer to the areas of the bottom Tee flange, bottom Tee web, top Tee flange and top Tee web respectively. y_{bTf}, y_{bTw}, y_{tTf} and y_{tTw} represent the distance between the top of the beam and the centroid of each of these areas. For the steel cellular beam, the position of the elastic neutral axis was calculated to be 375 mm from the top of the section, which is close to the value estimated during pouring of the concrete. The position of the elastic neutral axis for the composite section can be estimated in a similar way, by using an equivalent steel area for the concrete and a modular ration of 6 between the material stiffness values. Using the full area of the concrete, the elastic neutral axis is found to be 15 mm below the top of the beam. The position of the plastic neutral axis, following the guidelines of Eurocode 4 and using a plastic stress-block analysis with the design material strengths, was calculated to be located in the top Tee, 73 mm from the top of the beam. Using the actual material strengths the plastic neutral axis was calculated to be in the top Tee, at a distance of 88 mm from the top of the steel section. Therefore the approach using the applied load and analytical predictions indicates a higher position in the cross-section for both the elastic and plastic neutral axes than the position estimated from the measured strains and an assumed linear strain distribution.

From Figure 22, the difference in strain between the top flange of the steel (1702$\mu\varepsilon$) and the estimated strain on the bottom of the concrete slab (95$\mu\varepsilon$) indicates an interface slip of 1607$\mu\varepsilon$. If the magnitude of interface slip followed a cosine function along the beam length, this would result in a slip of 1607$\mu\varepsilon$×beam length/π = 7.8 mm at each end. This is slightly less than the measured slippage of 13.5 and 8.5 mm under the maximum load, suggesting that the strain distribution along the beam length is not exactly sinusoidal.

6.3 Vertical Deflection

The second moment of area of the unperforated steel beam before casting of the concrete was 758 × 10^6 mm^4 and this was reduced to 675 × 10^6 mm^4 at the centre of the opening. Based on the proportionate length of the openings, the effective second moment of area was found to be 734 × 10^6 mm^4 for the steel beam. The second moment of area of the composite section was calculated using a modular ratio of 6 between the stiffness of the steel and concrete and was found to be 2984 × 10^6 mm^4 for the unperforated beam and 2563 × 10^6 mm^4 at the centre of the opening. Based on the proportionate length of the openings, the effective second moment of area of the composite beam was found to be 2866 × 10^6 mm^4. The expected mid-span deflection δ for a beam subjected to uniformly distributed load w is given by

$$\delta = 5wL^4/384EI \tag{5}$$

where L is the span of the beam, E is the modulus of elasticity of the material and I is the second moment of area. As discussed previously, the load arrangement in the test consisted of 8 point loads, as shown in Figure 5, and the theoretical mid-span deflection under this loading arrangement is calculated as

$$\delta = 0.105PL^3/EI \approx 5.03wL^4/384EI \tag{6}$$

where P is one of the point loads, equivalent to $wL/8$. This differs from the uniformly distributed load case by 0.6 %. Both formulae were used to predict the deflection of the steel beam during pouring of the concrete and the deflections of the composite beam under each cycle of the uniformly distributed

load using the effective second moments of area, I_{eff}. The results are presented in Table 12 and compared with the vertical deflections measured during the tests, omitting the residual deflections from the previous loading cycles.

Table 12 Predicted and actual mid-length lateral deflections

Stage/Cycle	Load (kN/m^2)	I_{eff} (mm^4)	$\delta_{predicted,\ Eq(5)}$ (mm)	$\delta_{predicted,\ Eq(6)}$ (mm)	δ_{actual} (mm)
Concrete pour	2.7	734×10^6	37.1	37.3	38.0
1.0 × working load	5.0	2866×10^6	17.6	17.7	22.8
1.5 × working load	7.5	2866×10^6	26.4	26.6	35.2
2.4 × working load	12.0	2866×10^6	42.2	42.5	65.3
3.4 × working load	17.2	2866×10^6	60.5	60.9	142.6

The vertical deflection measured during the concrete pour was 38.0 mm, which was close to the predictions of 37.1 mm and 37.3 mm from Equations (5) and (6) respectively. The vertical deflection under 1.0 times the working load was 22.8 mm, which was slightly larger than the predicted deflection. The difference between the predicted and actual vertical deflections increased with each loading cycle, indicating the digression of the beam response from elastic behaviour. The predictions from Equation (6) were slightly closer to the experimental results than those from Equation (5). However, the difference between the predictions from the two equations was very small relative to the difference between the predicted and actual measured deflections and thus it can be concluded that the test set-up closely simulated uniformly distributed loading conditions.

6.4 Vierendeel bending

For the second test series described in Figure 13, an applied load P resulted in a maximum shear force of $5P/8$ acting on the beam with a shear force of $3P/8$ across the elongated opening. The resistance of the beam to Vierendeel bending at the elongated opening can be calculated following the approach of Lawson *et al*. [5]. Here, the effective length of the elongated opening, l_{eff}, is given by:

$$l_{eff} = l_0 - 0.5d_0 \quad (7)$$

where l_0 is the actual opening length and d_0 is the depth of the opening.

The total Vierendeel bending resistance is given by

$$M_v = 2M_{pt} + 2M_{pb} + M_{vc} \quad (8)$$

M_{pt} is the plastic bending resistance of the top Tee, M_{pb} is the plastic bending resistance of the bottom Tee and M_{vc} is the bending resistance due to composite action. A reduction factor is applied to M_{vc} to account for pull-out forces in the long opening, which is calculated as follows:

$$k_l = (1\text{-}l_{eff}/25h_t) \quad (9)$$

where h_t is the depth of the top Tee. Using the above equations, the effective length of the opening was found to be 893 mm and the bending resistance of the composite beam was estimated to be 93.2 kNm. The bending resistance corresponds to a shear resistance of 104.4 kN, which in turn corresponds to an applied load of 278.4 kN. This is considerably lower than the maximum applied load of 405 kN in the test. If the reduction factor k_1 is omitted, the resistance changes from 278.4 kN to 315.7 kN, which is still much lower than 405 kN.

The deflection data measured by LVDTs 2-7 (shown in Figure 13) during each cycle of the shear load test are presented in Figure 23.

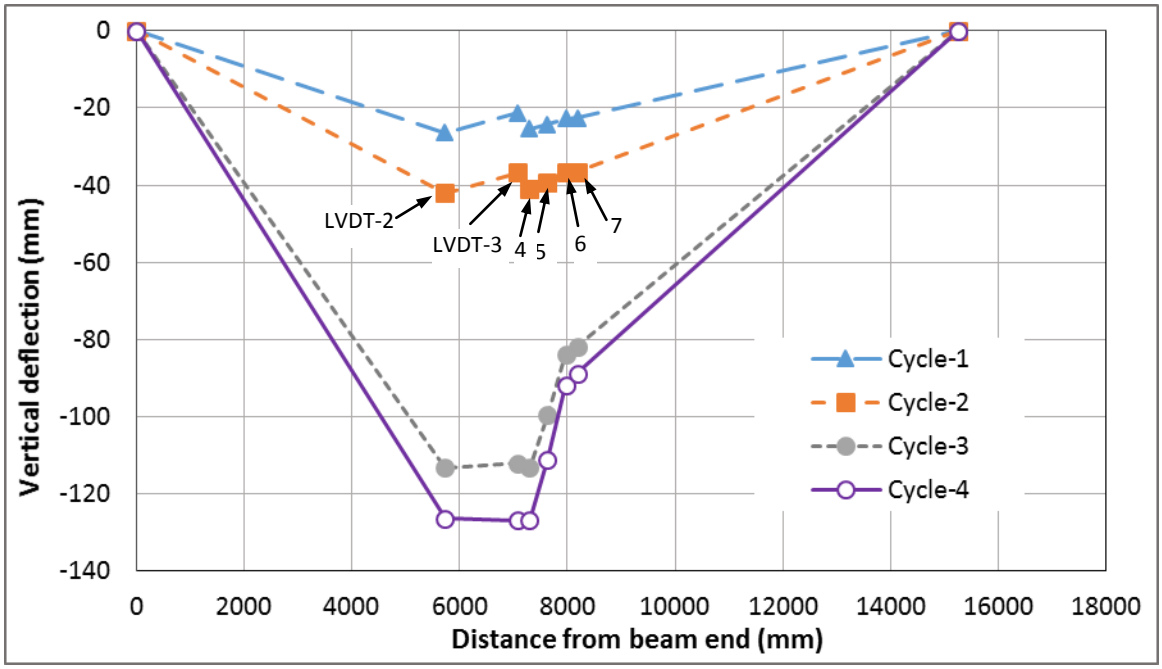

Figure 23 Deflection of beam during shear load test

If the deformed shape is idealized as a set of straight lines, connecting these points, then the largest rotations can be seen to occur at the locations of LVDT-2, where the shear load is applied, and LVDT-7, at the opposite end of the elongated opening, with smaller rotations occurring at the location of LVDTs 3, 4 and 6. Assuming that as the load is increased, plastic hinges eventually occur at each of these points, then the relationship between the applied load, deflection and rotations at the hinges can be described by

$$P\Delta_2 = \sum M_{p_i}\theta_i \tag{10}$$

where Δ_2 is the vertical displacement measured by LVDT-2, M_{pi} is the plastic moment resistance of the beam at the location of LVDT-i and θ_i is the rotation of the beam at the location of LVDT-i. Using the full cross-section plastic resistance at LVDT-2, M_{pt} for the top Tee at LVDTs 3 and 4, (M_{pt} + M_{vc}) for the top Tee at LVDTs 6 and 7, and M_{pb} for the bottom Tee at LVDTs 3, 4, 6 and 7, the estimated load required to cause the proposed plastic mechanism corresponding to each measured deflection Δ_2 is presented in Table 13:

Table 13 Estimated loads for plastic mechanism analysis

Cycle	Δ_2 (mm)	Load corresponding to plastic mechanism, P (kN)	Measured applied load (kN)
Cycle 1	26.4	647.0	107.7
Cycle 2	42	538.1	168.9
Cycle 3	113.3	364.0	387.8
Cycle 4	126.4	340.4	404.1

During the first 3 cycles, the full plastic moment has not been developed at the locations of the hinges, and the measured load is considerably lower than the estimated load corresponding to the plastic collapse mechanism. However, the measured applied load in the final cycles exceeds the load corresponding to the plastic collapse mechanism.

7 Conclusions

A series of experiments has been conducted to explore the response of an unpropped, long-spanning composite cellular beam with a low degree of shear connection. The beam has been tested under uniformly distributed loading and shear loading and the findings are summarised as follows:

- Under uniformly distributed loading, the beam resisted a maximum load of 3.4 × design working load prior to failure, despite having a degree of shear connection considerably below the minimum Eurocode 4 requirements outlined in Clause 6.6.1.2. This suggests that the rules for the minimum degree of shear connection could be relaxed.
- At the maximum uniformly distributed load, the bottom flange of the steel had reached yield, but the strains in the concrete were considerably lower than the failure strain. A reduced strain capacity in the bottom steel flange is to be expected for specimens using unpropped construction. However, the overall resistance of the beam exceeded the design expectations, demonstrating the suitability of unpropped construction methods for composite beams.
- Ductile behaviour of the shear connectors was confirmed by the observed end slips of 8.5 mm and 13.5 mm under uniformly distributed loading, which exceeded the minimum of 6 mm specified in

Eurocode 4 Clause 6.6.1.1. Although bending was observed in some connectors located close to the end supports, no shear connector failed during the two series of tests.

- A mid-span vertical deflection of $L/100$ served as a suitable criterion for failure, as evidenced by the reduced load and excessive deflections that occurred in the subsequent loading cycle. However, since this corresponded to a maximum load of 17.2 kN/m^2, recommendations for the working design load of composite beams could be revised to better utilise the merits of cellular asymmetric beams that employ unpropped construction. The load-deflection behaviour was linear up to 7.5 kN/m^2, with little residual deflection observed upon unloading at this stage of the test.
- In the shear load test, the beam withstood a maximum applied point load of 405 kN, which was 45% higher than the predicted resistance of the steel cross-section. Neglecting the reduction factor applied to account for pull-out forces, the bending maximum load would still exceed the predicted load by 28%. This suggests the need for modifications to the predicted Vierendeel bending resistance for composite cellular beams.
- The vertical deflections of the beam were underestimated by the equation $\delta = 5wL^4/384EI$. Further provisions are needed to predict the deflection of composite cellular beams for serviceability.

The findings suggest that Eurocode 4 design recommendations could be modified to better exploit the properties of unpropped composite cellular beams, particularly with regard to the required degree of shear connection. Further test data is needed to verify these results, and this will be obtained through future experiments within the "DISCCO" project. Numerical analysis using finite element software will also support the recommendations following from this research project.

8 Acknowledgement

The research covered in this paper is part of a collaborative project between the Steel Construction Institute, the University of Stuttgart, the University of Luxembourg, ArcelorMittal and the University of Bradford, and is funded by the European Community's Research Fund for Coal and Steel under grant agreement no. RFSR-CT-2012-00030 who is gratefully acknowledged. The authors also would

like to thank technicians at the School of Engineering, University of Bradford and PhD candidates Ms Jie Yang, Mr Naveed Rehman and Mr Sahr Thomas Gbatta for their assistance with the tests.

References

[1] Ranzi G, Bradford MA, Ansourian P, Filonov A, Rasmussen KJR, Hogan TJ and Uy B. Full-scale tests on composite steel-concrete beams with steel trapezoidal decking. J Constr Steel Res 2009; 65(7): 1490-1506.

[2] Lam D. Capacities of headed stud shear connectors in composite steel beams with precast hollowcore slabs. J Constr Steel Res 2007; 63(9): 1160-74.

[3] Erdal F and Saka MP. Ultimate load carrying capacity of optimally designed steel cellular beams. J Constr Steel Res 2013; 80: 355-68.

[4] Chung KF, Liu TCH and Ko ACH. Investigation on Vierendeel mechanism in steel beams with circular web openings. J Constr Steel Res 2001; 57(5): 467-90.

[5] Lawson RM, Lim J, Hicks SJ and Simms WI. Design of composite asymmetric cellular beams and beams with large web openings. J Constr Steel Res 2006 62(6): 614-29.

[6] ECSC project P4383. Large web openings for service integration in composite floors (LWO) 2003.

[7] EN 1994-1-1. Eurocode 4. Design of composite steel and concrete structures – Part 1-1: General rules and rules for buildings; 2004.

[8] Lawson RM. and Saverirajan AHA. Simplified elasto-plastic analysis of composite beams and cellular beams to Eurocode 4. J Constr Steel Res 2011; 67(10): 1426-34.

[9] Banfi, M. Slip in composite beams using typical material curves and the effect of changes in beam layout and loading, Engineering Foundation Conference V, South Africa 2005.